Available online at www.sciencedirect.com
ScienceDirect
Solar Energy Materials & Solar Cells
ELSEVIER
Solar Energy Materials & Solar Cells 90 (2006) 2855–2866
www.elsevier.com/locate/solmat

Investigation of rapid thermal annealing on $Cu(In,Ga)Se_2$ films and solar cells

Xuege Wang[a], Sheng. S. Li[a,*], W.K. Kim[b], S. Yoon[b], V. Craciun[c], J.M. Howard[c], S. Easwaran[d], O. Manasreh[d], O.D. Crisalle[b], T.J. Anderson[b]

[a]*Department of Electrical and Computer Engineering, University of Florida, Gainesville, FL 32611, USA*
[b]*Department of Chemical Engineering, University of Florida, Gainesville, FL 32611, USA*
[c]*Department of Material Science and Engineering, University of Florida, Gainesville, FL 32611, USA*
[d]*Department of Electrical Engineering, University of Arkansas, Fayetteville, AR 72701, USA*

Received 10 August 2005; received in revised form 10 April 2006; accepted 17 April 2006
Available online 10 July 2006

Abstract

Rapid thermal annealing (RTA), with fast ramp rate, was performed on several $Cu(In,Ga)Se_2$ (CIGS) films and solar cells under various peak annealing temperatures and holding times. Characterizations were made on CIGS films and cells before and after RTA treatments to study effects of RTA on the CIGS film properties and cell performance. In addition, AMPS-1D device simulation program was used to study effects of defect density on the cell performance by fitting the experimental data of RTA-treated CIGS cells. The results show that RTA treatments under optimal annealing condition can provide significant improvements in the electrical properties of CIGS films and cell performance while preserving the film composition and microstructure morphology.

Keywords: Rapid thermal annealing (RTA); $Cu(In,Ga)Se_2$ (CIGS); Hall effect

1. Introduction

Rapid thermal annealing (RTA) at higher temperatures with a low thermal budget has been widely used in thin film manufacturing industry to activate doping impurities while at

*Corresponding author. Tel.:/fax: +1 35 23924937.
E-mail address: shengli@eng.ufl.edu (S.S. Li).

0927-0248/$ - see front matter © 2006 Elsevier B.V. All rights reserved.
doi:10.1016/j.solmat.2006.04.011

the same time minimizing the doping impurity diffusion that occurs during thermal processing [1–12]. As a powerful annealing technique, the RTA process offers several advantages such as short cycle time, reduced thermal exposure and lot size flexibility compared to conventional furnaces. In general, RTA improves the temperature uniformity for large-diameter wafers over the conventional furnace heating. Strong demand in thermal budget reduction and cycle time reduction makes RTA treatment a very popular thermal processing method for semiconductor device processing in recent years. The RTA technique has been successfully applied to the fabrication of low-cost silicon solar cells. The motivation of using this technique on $Cu(In,Ga)Se_2$ (CIGS) films and solar cells is to reduce damages and defect densities in the near-surface junction region, which tends to reduce the losses due to recombination via defect centers in the junction space charge region, and hence improves the cell performance.

2. Fabrication details

The CIGS samples grown on the Mo-coated soda-lime glass (SLG) substrates were prepared by the National Renewable Energy Lab (NREL), Shell Solar Industry (SSI) and Energy Photovoltaics Inc. (EPV), which were used in this work to study the effects of RTA treatments on the CIGS film properties and cell performance. For the Hall-effect measurements, however, the CIGS films were grown directly on the insulating SLG substrates. To study the effects of RTA treatments on CIGS device performance, a thin (50 nm) CdS buffer layer was first deposited on the CIGS samples by chemical bath deposition (CBD) method. ZnO window layer was then deposited on the CdS/CIGS/Mo/SLG samples by RF sputtering. Subsequent metallization (using Ni–Al front contact grids) was carried out by e-beam evaporation through a shadow-mask. Finally, finished devices were produced by cutting these CIGS samples into separate cells, and wires were attached using indium-bumps on the Mo-coated SLG substrates for back contacts. In this study, conditions of RTA treatments on CIGS films and cells were varied from 100 to 350 °C with different holding time and ambient.

3. Effects of RTA on CIGS film properties

Five 1×1 in CIGS samples (from SSI) grown on the Mo-coated SLG substrates were cut from a large CIGS sample. Four CIGS samples were treated with RTA under different annealing conditions (see Table 1), and one control sample received no RTA treatment. The XRD and SEM surface characterizations were performed on all five samples. The XRD analyses provide information about the preferred film orientation and composition.

Table 1
RTA conditions of SSI-CIGS samples

Sample #	F-R1	F-R2	F-R3	F-R4
RTA (°C)	300	300	350	350
Holding (s)	60	120	60	120
Ramp up rate (°C/s)	25	25	25	25
Ramp down rate (°C/s)	10	10	10	10
Ambient	Ar	Ar	Ar	Ar

The SEM photos reveal the surface morphology and grain size. Little or no changes among the RTA samples and control sample were observed from the XRD and SEM results shown in Figs. 1 and 2. Only some slightly blurry grain edges were observed in the SEM images for the two samples treated at 350 °C (sample #F-R3 and F-R4) as compared to the 300 °C RTA-treated samples and control sample. These suggest that the overall film composition and surface morphology do not change during the RTA treatments.

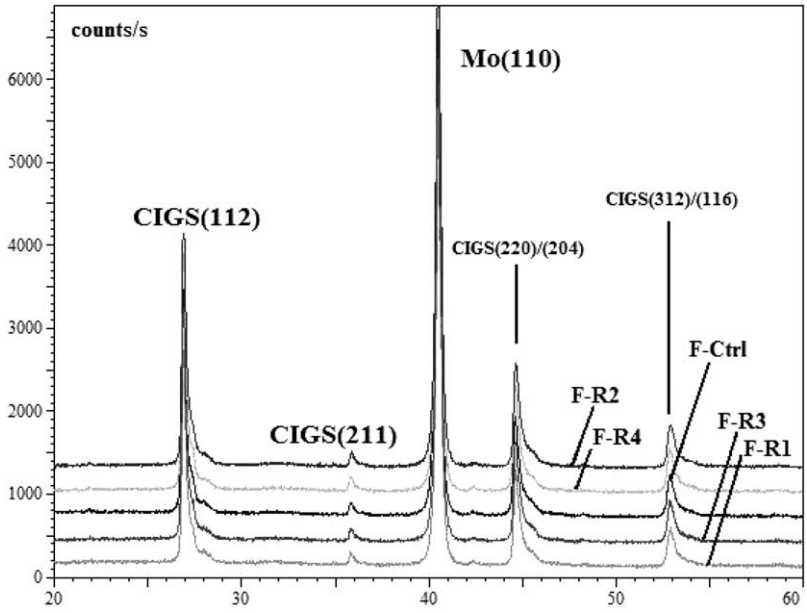

Fig. 1. XRD results of RTA-treated SSI-CIGS films and the control sample.

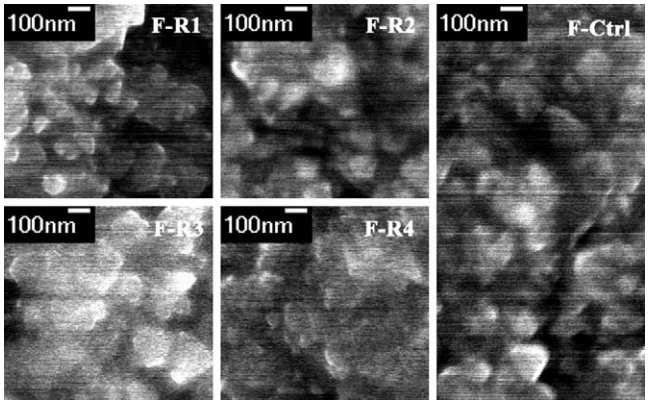

Fig. 2. Surface morphology of RTA-treated SSI-CIGS films and the control sample. (SEM images with a magnification of 30,000 × .)

In order to determine the effects of RTA treatments on the carrier concentration, carrier mobility and sheet resistance of CIGS films, the resistivity and Hall-effect measurements were carried out on two NREL-CIGS films directly deposited on the SGL substrates before and after RTA treatments. The annealing conditions and the results of resistivity and Hall-effect measurements (using an MMR Hall- and Van Der Pauw-measurement system [13,14]) before and after the RTA treatments are summarized in Table 2.

The Hall-effect measurements show a significant increase of hole density and a decrease in film resistivity, Hall coefficient and sheet resistance following the RTA treatment. For sample #H300-1, which was treated by 300 °C RTA, the carrier mobility after RTA was found 2 times larger than the value before annealing, while for sample #H350-1, which was treated by 350 °C RTA, the hole mobility was dropped by more than 50% after the RTA treatment. The results revealed that 350 °C RTA increased the carrier concentration by nearly two orders of magnitude, which also led to the decrease of carrier mobility. The 300 °C RTA-treated sample showed beneficial results on the film resistivity, carrier mobility and carrier density. Therefore, the peak annealing temperature plays an important role in determining the electrical properties of RTA-treated CIGS absorber layers.

3.1. Progressive RTA treatments on CIGS solar cells

The progressive RTA experiments were performed on one CIGS device, which contains three cells (provided by NREL). The basic sequence of the progressive RTA treatment is given as follows:

- Prepare the CIGS device.
- Measure the photo-J–V performance before RTA.
- Perform the RTA on CIGS cells at 100 °C for 30 s.
- Measure the photo-J–V performance after RTA.
- Anneal the CIGS cells at 200 °C for 30 s by RTA.
- Measure the photo-J–V performance again.
- Perform the RTA at $T = 300$ °C or higher for 30 s, and measure the photo-J–V again.

Table 2
Hall-effect data of NREL-CIGS samples before and after RTA treatments

	Sample #H300-1	Sample #H350-1
RTA condition	300 °C, 1 min	350 °C, 1 min
Ramp up rate	25 °C/s	25 °C/s
Ramp down rate	10 °C/s	10 °C/s
Ambient	Ar	Ar
Resistivity (Ω-cm)[a]	70.58/4.21	55.76/2.17
Mobility (cm^2/Vs)[a]	2.80/6.77	4.28/1.86
Hole density (cm^{-3})[a]	$3.16 \times 10^{16}/2.19 \times 10^{17}$	$2.62 \times 10^{16}/1.55 \times 10^{18}$
Hall coefficient (cm^3/Coul)[a]	197.77/28.48	238.53/4.03
Sheet resistance (Ω/cm^2)[a]	470536.4/28044.4	371761.8/14435.8
Carrier type	Holes/holes	Holes/holes

[a]Data taken before/after RTA treatments.

- Continue increasing the annealing temperature of each RTA until the cell performance drastically drops or cells were destroyed.

The photo-J–V results show that progressive RTA treatment (in N_2 ambient) could significantly improve the cell performance and overall uniformity of large-area CIGS solar cells. As shown in Table 3, significant improvements in open-circuit voltage (V_{oc}), short-circuit current density (J_{sc}), fill factor (FF) and conversion efficiency (Eff) were observed in all three cells after each progressive RTA treatment at temperatures of 100, 200 and 300 °C for 30 s. A dramatic increase in the conversion efficiency of cell #1 (bad cell) from 9.52% to 15.77% AM1.5G shows that the progressive RTA treatment could be used to enhance the structure uniformity and the overall performance of large-area cells.

We also applied 400 °C RTA treatment on the same CIGS sample; unfortunately, the whole device, which contains the three CIGS cells discussed above, was destroyed. Therefore, the only experimental data we have on these cells are the values of V_{oc}, J_{sc}, FF and Eff measured before and after each progressive RTA up to 300 °C. In order to extract other important parameters of these cells, the device modeling and simulation of these cells were also carried out using the AMPS-1D (Analysis of Microelectronic and Photonic Structures) device simulation program [15]. The main objective of this simulation is to study the effect of defect density on the CIGS cells before and after each progressive annealing, and to extract the dark-J–V and quantum efficiency (Q–E) data. The device modeling and simulation results are discussed later.

Table 3
Photo-J–V results of NREL-CIGS solar cells before and after progressive RTA

	Cell #1	Cell #2	Cell #3
Pre-annealing			
V_{oc} (V)	0.628	0.652	0.655
J_{sc} (mA/cm^2)	31.66	32.97	33.50
FF (%)	47.88	68.52	70.71
Eff (%)	9.52	14.73	15.51
100 °C RTA			
V_{oc} (V)	0.633	0.656	0.660
J_{sc} (mA/cm^2)	34.30	35.47	34.05
FF (%)	56.81	71.10	73.03
Eff (%)	12.32	16.55	16.19
200 °C RTA			
V_{oc} (V)	0.652	0.657	0.650
J_{sc} (mA/cm^2)	34.85	35.11	32.34
FF (%)	68.43	72.14	76.15
Eff (%)	15.55	16.65	16.01
300 °C RTA			
V_{oc} (V)	0.627	0.623	0.630
J_{sc} (mA/cm^2)	35.39	36.35	35.08
FF (%)	71.05	70.48	74.32
Eff (%)	15.77	15.96	16.42

Note: in N_2 ambient, 30-s holding time, ramp up rate = 60°C/s.

4. RTA effects of separated CIGS solar cells

Six CIGS solar cells from SSI and EPV were treated by RTA under different annealing conditions. The performance of these cells was then tested by using dark-J–V, photo-J–V and Q–E measurements before and after RTA treatments under different annealing conditions. The annealing condition and photo-J–V results of these RTA-treated solar cells are summarized in Table 4.

For cell #R1 which was treated at lowest RTA temperature (100 °C), the FF and Eff were improved after RTA. For cell #R2 treated at 150 °C RTA, the overall performance was improved explicitly after RTA (see Fig. 3). Under high-temperature RTA condition ($T \geqslant 300$ °C), for cells #R3, #R4 and #R6, we found that V_{oc}, J_{sc} and Eff increased, while FF decreased after RTA treatment. For cell #R4, which was annealed at the highest peak temperature (350 °C) and longest holding time (2 min), only J_{sc} increased after RTA and the overall performance dropped. By taking a closer look at the FF data of four SSI cells,

Table 4
Photo-J–V results of separated CIGS solar cells before and after RTA

Cell #	R1	R2	R3	R4	R5	R6
Source	EPV	EPV	SSI	SSI	SSI	SSI
RTA (°C)	100	150	300	300	350	350
Holding (s)	30	30	60	120	60	120
Ambient	He	He	Air	Air	Air	Air
V_{oc} (V)[a]	0.500/0.503	0.430/0.509	0.455/0.471	0.471/0.487	0.465/0.471	0.465/0.422
J_{sc} (mA/cm^2)[a]	24.74/24.68	25.56/28.85	27.49/31.43	26.55/30.51	28.75/33.94	27.67/30.41
FF (%)[a]	61.45/67.60	45.91/51.90	52.69/49.01	57.48/49.96	52.14/48.58	48.00/39.36
Eff (%)[a]	8.190/8.350	5.030/7.620	6.591/7.259	7.196/7.422	6.975/7.759	6.177/5.051

[a]Data taken before/after RTA treatments.

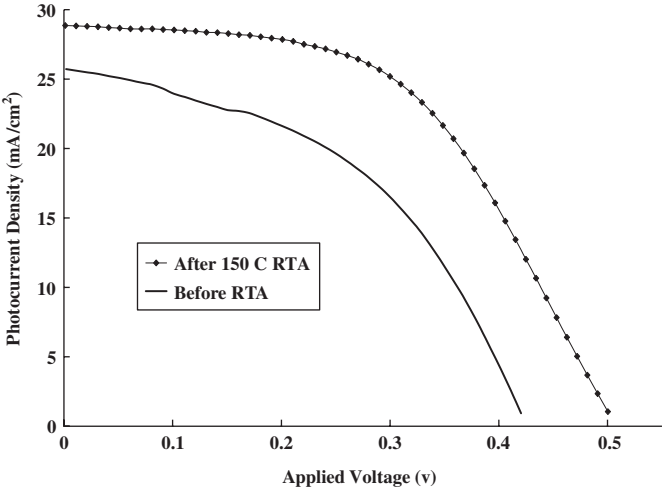

Fig. 3. Photo-J–V curves of tested CIGS solar cell (#R2) before and after RTA (150 °C, 30 s) treatment.

we found that for the cell treated by 2-min RTA, the FF dropped more than that of the cell treated by 1-min RTA at the same temperature. This suggests that 1 min is enough for the RTA treatment, and too long holding time can degrade the performance. Comparing four SSI cells with two EPV cells and the progressive RTA cells (NREL), it was also found that using inert gas (N_2 or He) ambient yielded better results for RTA treatment on CIGS cells.

From the dark-J–V results, we found that the overall dark current density decreased in the forward bias region for the four SSI cells (#R3–#R6) after high-temperature RTA treatment. Though the dark current density decreased after RTA, the shape of the J–V curves after RTA tends to become linear (see Fig. 4), which suggests that the resistivity decreases during the RTA and hence results in FF loss (see Table 4). For cells #R1 and #R2, which were treated by low-temperature RTA, slight decrease of dark current density was also observed after RTA and the shape of J–V curves remains the same as before the RTA treatment. One possible reason of FF loss for the high-temperature RTA ($T \geqslant 300\,^{\circ}C$) cells is the low melting point of indium contact (156.61 °C). For RTA cells treated by temperature higher that than point, indium diffusion from the back contact might cause the decrease of the resistivity and the FF. This may explain why no FF loss was observed for cells #R1 and #R2, which were treated by low-temperature RTA ($T \leqslant 150\,^{\circ}C$). Also the higher possibility of selenium loss from the CIGS layer under high temperature RTA might create more shunt in the junction region and hence decrease the FF.

From the measured Q–E results, improvements on Q–E were observed over the entire wavelength region of interest for all the tested cells after RTA treatments, which suggest RTA has positive effect on all layers (absorber layer, buffer layer and window layer) of CIGS solar cells. These results are consistent with the photo-J–V results showed before; even for cell #R6 (Fig. 5) which has an overall decrease in photo-J–V performance after RTA, the Q–E still showed that photo current density in the interested wavelength region was increased after RTA treatment.

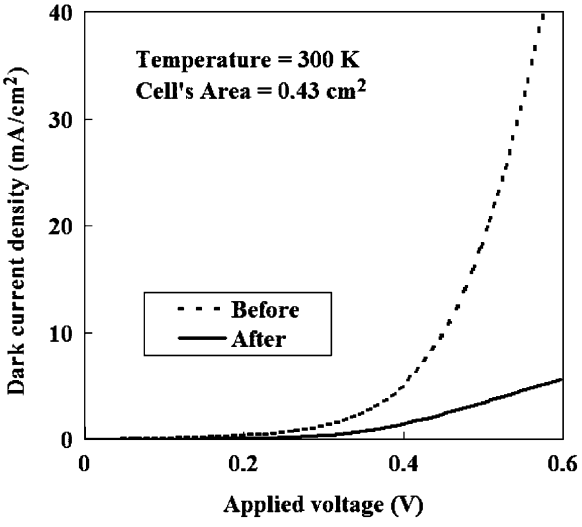

Fig. 4. Dark-J–V curves of tested CIGS solar cell (#R4) before and after RTA (300 °C, 120 s) treatment.

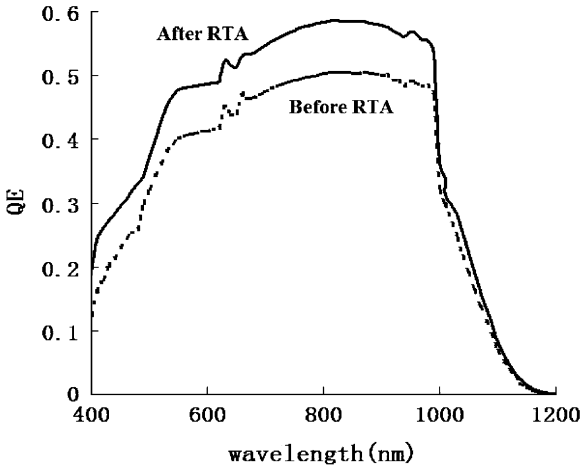

Fig. 5. Q–E curves of tested CIGS solar cell (#R6) before and after RTA (350 °C, 120 s) treatment.

5. Device simulation

The objective of this study is to analyze the performance of CIGS cells versus the defect density in the CIGS absorber layer, and to fit the experimental photo-J–V data by using solar cell simulation program, and extract the cell parameters which could not be obtained from the damaged device experimentally.

The CIGS solar cell structure used in this simulation consists of a 155 nm ZnO ($E_g = 3.3$ eV) TCO layer, a 51 nm CdS ($E_g = 2.4$ eV) buffer layer; an ultra-thin high-recombination interface layer ($E_g = 1.5$ eV) with a high density of effective recombination centers placed at the metallurgical junction between the CIGS surface layer and CdS buffer layer; an inverted n-type surface layer [16,17] with a thickness of 60 nm, net carrier density $n = 3 \times 10^{12}\,\mathrm{cm}^{-3}$, a band-gap energy, $E_g = 1.3$ eV, is inserted between the CdS and CIGS layers; and finally the CIGS ($CuIn_{0.68}Ga_{0.32}Se$) absorber layer with a band-gap energy of $E_g = 1.2$ eV. The total thickness of the absorber layer is assumed equal to 2 μm for all simulation cases in this study. The computer simulation tool AMPS-1D is employed by specifying the semiconductor parameters (e.g., carrier mobility and carrier concentration from Hall-effect measurements) in each defined layer of the cell structure as input parameters in the simulation. In this study, the defect density of CIGS absorber is varied from 1×10^{14} to $1 \times 10^{19}\,\mathrm{cm}^{-3}$, with other parameters kept unchanged. The results shown in Fig. 6 reveal that the cell performance is nearly unchanged for defect density below $2 \times 10^{16}\,\mathrm{cm}^{-3}$. Above this value, V_{oc}, J_{sc} and Eff start dropping with the increase of defect density, which suggests that to gain an optimal device performance, the defect density should be less than $2 \times 10^{16}\,\mathrm{cm}^{-3}$. It is also found that the defect density does not affect the FF value in the simulations.

An excellent fit of the experimental J–V data was next obtained from the simulation. In the progressive RTA study, the most significant performance improvement occurs on cell #1 (bad cell), and other cells only showed a slight increase in the photo-J–V parameters (see Table 3). Therefore, the simulation was focused on fitting the progressive RTA data in

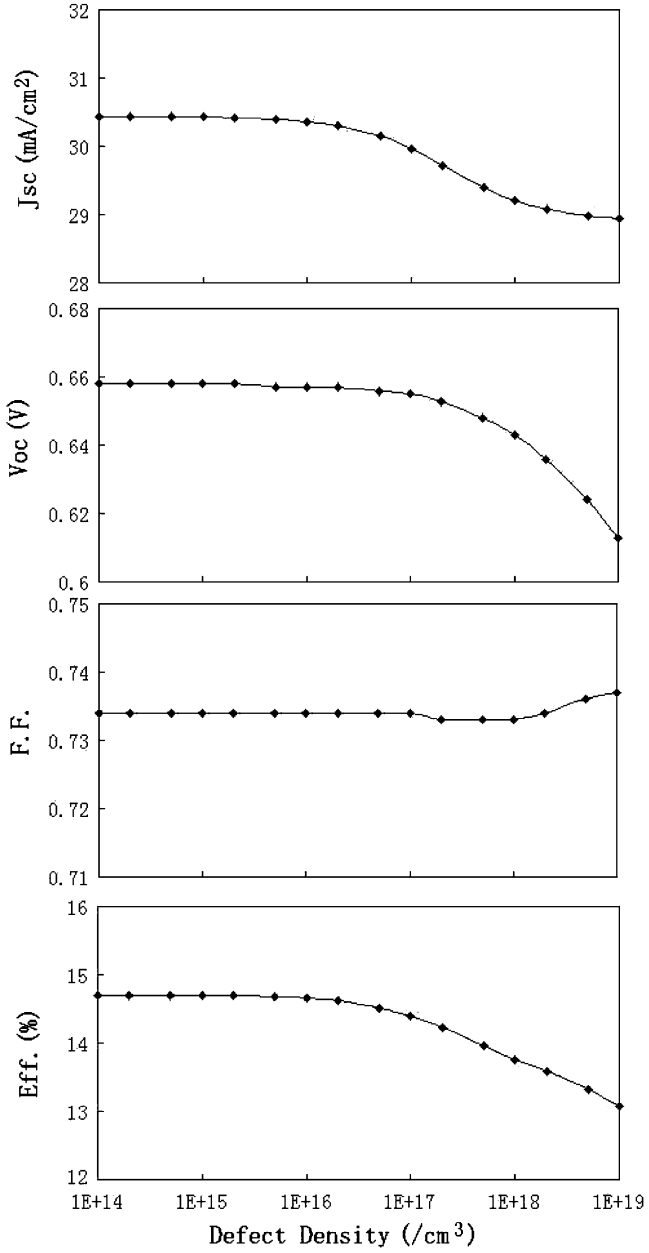

Fig. 6. Performance parameters of CIGS ($E_g = 1.2$ eV) solar cells versus defect density of CIGS absorber layer.

cell #1. By mainly varying the defect density, carrier concentration and mobility of the CIGS absorber layer, along with minor adjustment of some parameters in ZnO TCO and CdS buffer layers, a good agreement between the experimental data and the simulation results of cell #1 before and after progressive RTA was obtained, as shown in Table 5. The simulation results show that defect density of CIGS layer decreased from 4×10^{17} to

Table 5
Photo-J–V data of cell ♯1 before and after progressive RTA treatment (from experiment and AMPS-1D simulation results)

	Before	100 °C	200 °C	300 °C
V_{oc} (V)[a]	0.628/0.6282	0.633/0.6331	0.652/0.6525	0.627/0.6318
J_{sc} (mA/cm^2)[a]	31.66/31.64	34.30/34.30	34.85/34.796	35.39/35.392
FF (%)[a]	47.88/46.8	56.81/56.8	68.43/68.2	71.05/71.5
Eff (%)[a]	9.520/9.647	12.32/12.276	15.55/15.409	15.77/15.763
Defect density (cm^{-3})[b]	4×10^{17}	1×10^{17}	3×10^{16}	1×10^{16}

[a]Data obtained from experiment/simulation.
[b]Data obtained from simulation only.

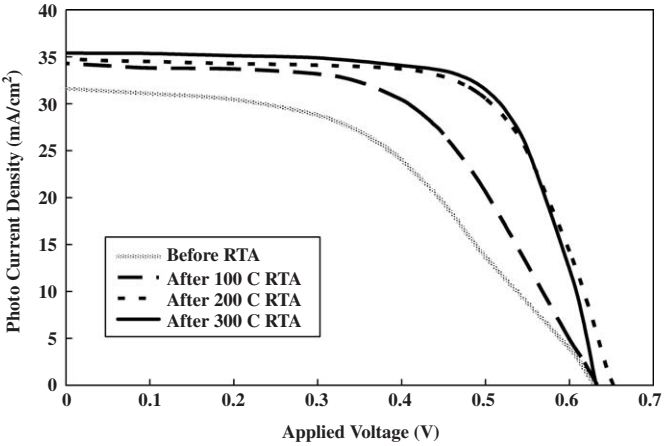

Fig. 7. Photo-J–V curves of cell #1 before and after progressive RTA treatment (from AMPS-1D simulation results).

$1\times10^{16}\,\mathrm{cm}^{-3}$ after three consecutive progressive RTA treatments, which suggest that progressive RTA might provide an effective means to reduce the defect density in CIGS solar cells. Fig. 7 shows the photo-J–V curve of cell #1 before and after each progressive RTA treatment from the simulation results. To extract other device parameters, data of the dark current and spectral response were obtained from the simulation. Fig. 8 shows the dark-J–V plots of cell #1 before and after each progressive RTA treatment. We observed that in the high forward bias regime with voltage greater than 0.88 V, the dark-J–V curves after each progressive RTA were found to be apparently lower than data before RTA. These results suggest that RTA under certain annealing conditions could reduce the defect density and hence decrease the recombination current in the device. Fig. 9 shows the Q–E curves before and after progressive RTA treatments, explicitly the Q–E curves after each progressive RTA are higher than data before the RTA. Since only the defect parameters were adjusted in the CIGS absorber layer in this simulation study, the noticeable Q–E improvement in each progressive RTA treatment occurs only for photon wavelengths greater than ~580 nm.

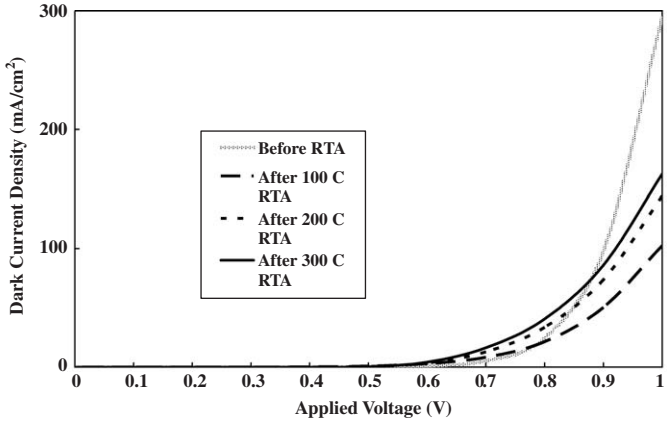

Fig. 8. Dark-J–V curves of cell #1 before and after progressive RTA treatment (from AMPS-1D simulation results).

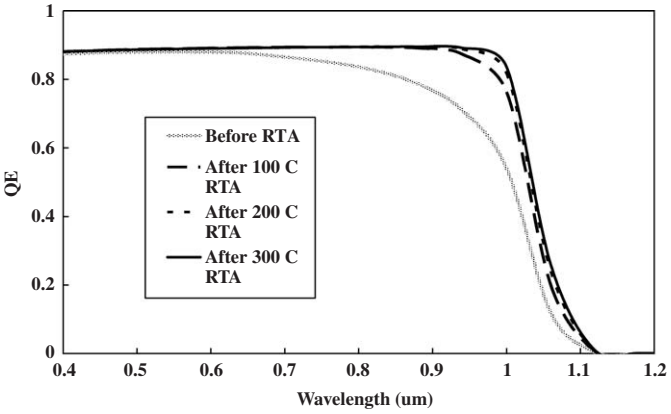

Fig. 9. Q–E plots of cell #1 before and after progressive RTA treatments (from AMPS-1D simulation results).

6. Conclusions

In this study, we have shown that progressive RTA treatments can significantly improve the performance and overall uniformity of large-area CIGS solar cells. Using low-temperature ($T \leqslant 300\,^{\circ}\mathrm{C}$) RTA treatment, improvements were observed on the carrier concentration and mobility, and film resistivity while the surface composition and morphology remain unchanged. The estimated optimal annealing temperature for the CIGS films and cells should be around 200 °C with less than 1 min holding time in inert gas ambient. Simulation study of defect density versus CIGS device performance shows cell performance starting to drop for defect densities greater than $2 \times 10^{16}\,\mathrm{cm}^{-3}$, and no strong correlation between the defect density and FF was found. Excellent fitting of the progressive RTA data was also obtained by AMPS-1D simulation, and the results suggest that progressive RTA treatment can reduce the defect density in CIGS absorber layer and hence improve the photo-J–V, dark-J–V and spectral response of the cell. Future efforts

should focus on investigating the optimal annealing condition using different RTA systems on CIGS solar cells.

Acknowledgments

This work was supported by the US Department of Energy/National Renewable Energy Laboratory (DOE/NREL) Thin Film Photovoltaic Partnership Program (TFPPP) under Contract no.ADJ-2-30630-13. The authors would like to thank Drs. Von Roedern Bolko and Rommel Noufi of NREL for their interest and support of this work. The author also would like to thank Dr. Dale Tarrant of SSI and Dr. Leon Chen of EPV, for the supply of CIGS samples used in this study.

References

[1] R. Kakkad, G. Liu, S.J. Fonash, J. Non-Cryst. Solids 115 (1989) 66.
[2] G. Liu, S.J. Fonash, Appl. Phys. Lett. 55 (7) (1989) 660.
[3] G. Liu, S.J. Fonash, Appl. Phys. Lett. 62 (20) (1993) 2554.
[4] S. Bae, S.J. Fonash, Appl. Phys. Lett. 76 (5) (2000) 595.
[5] A.K. Kalkan, S.J. Fonash, J. Electrochem. Soc. 144 (11) (1997) L297.
[6] S.Y. Yoon, K.H. Kim, C.O. Kim, J.Y. Oh, J. Jang, J. Appl. Phys. 82 (11) (1997) 5865.
[7] C. Hayzelden, J.L. Batstone, J. Appl. Phys. 73 (12) (1993) 8279.
[8] W.K. Loke, S.F. Yoon, S.Z. Wang, T.K. Ng, W.J. Fan, J. Appl. Phys. 91 (8) (2002) 4900.
[9] X. Zhang, T. Zhang, M. Wong, Y. Zohar, J. Microelectromech. Syst. 7 (4) (1998) 356.
[10] S.J. Xu, X.C. Wang, S.J. Chua, C.H. Wang, W.J. Fan, J. Jiang, X.G. Xie, Appl. Phys. Lett. 72 (22) (1998) 3335.
[11] S.J. Wang, C.K. Ong, Semicond. Sci. Technol. 18 (2003) 154.
[12] M. Izadifard, I.A. Buyanova, J.P. Bergman, W.M. Chen, A. Utsumi, Y. Furukawa, A. Wakahara, H. Yonezu, Semicond. Sci. Technol. 20 (2005) 353.
[13] L.J. Van Der Pauw, Philips Tech. Rev. 20 (1958) 220.
[14] L.J. Van Der Pauw, Philips Res. Rep. 13 (1958) 1.
[15] H. Zhu, A.K. Kalkan, J. Hou, S.J. Fonash, Am. Inst. Phys. Conf. Proc. 462 (1999) 309.
[16] D. Schmid, D.M. Ruckh, F. Grunwald, H.W. Schock, J. Appl. Phys. 73 (6) (1992) 2902.
[17] M.A. Contreras, H. Wiesner, D. Niles, K. Ramanathan, R. Matson, J. Tuttle, J. Keane, R. Noufi, in: Conference Record of the 25th IEEE Photovoltaic Specialists Conference, 1996, pp. 809–812.